Study on the synergistic anticorrosion property of a fully bio-based polybenzoxazine copolymer resin

Yitong Zhang[a], Xiaoyun Liu[a],*, Guozhu Zhan[b], Qixin Zhuang[a], Ruhong Zhang[a], Jun Qian[a],*

[a] The Key Laboratory of Advanced Polymer Materials of Shanghai, School of Materials Science and Engineering, East China University of Science and Technology, Shanghai 200237, China
[b] The 806th Institute of the Eighth Academy of CASC, Huzhou 313000, China

ABSTRACT

In this paper a novel bio-based benzoxazine, dehydroabietylamine benzoxazine monomer (D-Bz), was synthesized and a series of copolymers were prepared by using D-Bz and two other bio-based benzoxazines 6-allyl-8-methoxy-3-octadecyl-3, 4-dihydro-2H-benzoxazine (S-Bz) and 6-allyl-3 –(furan-2-ylmethl)-8-methoxy-3, 4-dihydro-2H-benzoxazine (F-Bz). The structure, morphology and curing process are characterized by ^{1}H nuclear magnetic resonance spectroscopy (^{1}H NMR), mass spectrometry (MS), fourier transform infrared spectroscopy (FTIR), scanning electron microscope (SEM), differential scanning calorimetry (DSC) and thermogravimetric analysis (TGA). Electrochemical techniques such as open circuit voltage time (OCPT), Tafel and electrochemical impedance spectra (EIS) were used to study their electrochemical corrosion properties. Results show that among these copolymer, when the ratio of S-Bz: D-Bz: F-Bz is 1:6:3, the copolymer has good synergistic effects, showing a lower dielectric constant (2.47 at 1000 Hz), higher crosslink density ($5.29 \ast E^{-4}$ mol/ml), lower corrosion current ($0.030 \, \mu A/cm^2$) and the best electrochemical corrosion efficiency (99.73%).

1. Introduction

Corrosion is the destruction and deterioration of materials caused by the reaction of materials with their environment; it is the main factor causing the failure of metal materials. Corrosion has adverse impacts on the chemical, shipping, manufacturing and architectural industries [1,2]. One of most widely used methods to mitigate corrosion is polymer coatings which provide a physical barrier against corrosion [3–5]. These physical barriers prevent oxygen, water and corrosive ions from coming into contact with the metal substrate in order to protect from corrosion [6,7].

At present, there are many kinds of polymers used in anti-corrosion coatings, among which epoxy resin [8,9], polyaniline [10,11], phenolic resin [12] and the like have been studied. Of these polymers, phenolic resins are widely used as binders and coatings due to their high mechanical strength, excellent thermal stability and chemical resistance [13,14].

A new type of thermosetting phenolic resin, benzoxazine resin, have highly exceptional properties, such as excellent chemical resistance, thermal stability, high char yield, very long shelf life [15,16]. In addition, Polybenzoxazine resin (PBz) has shown other excellent properties, such as low water absorption, near-zero shrinkage, low surface free energy and dielectric properties [17–28]. PBz has been studied as an anti-corrosion coating [16,29–34], shown to inhibit the corrosion of coated steel samples due to the formation of a stable network that diminished the permeability of corrosion agents to the metallic substrate [35–39]. Lin et al. mixed blends possessing a maleimide-containing benzoxazine compound (MI-Bz) and an amine-capped aniline trimer (ACAT) [30]. Lin's study found that a covalent bond was established between the ACAT and MI-Bz compounds which had a synergistic effect on their respective anticorrosion properties. Caldona et al. adopted rubber-modified PBz as an anti-corrosion coating for low carbon steel [31]. Electrochemical measurements recorded after immersion in chloride solution showed that the rubber-modified PBz was able to protect the carbon steel from corrosion attack due to its slow surface energy properties and water resistance ability (contact angle: CA = 101°). The electrochemical corrosion protection efficiency is about 92%. Most studies on the corrosion protection of PBz coated metals look at the homopolymer or composite; however, the preparation of composite materials also requires consideration of the compatibility and dispersion of the applied filler particles [31]. Therefore, it is necessary to study the synergistic effects of different PBz coatings on corrosion resistance.

Nowadays, inspired by environmental protection policies, the use of

renewable resources as chemical raw materials has become an important topic for researchers in various fields. Bio-based materials have the advantages of being 'green', environmental friendliness, and resource-saving. Renewables are gradually becoming a leading industry that guides scientific and technological innovation and economic development [37–39]. Our research group has previously reported two novel bio-based benzoxazines, obtained from rosin (Dehydroabietylamine), which have high corrosion resistance and an electrochemical corrosion protection efficiency of 83% [40]. The materials also have a stable open circuit voltage time in corrosion resistance and low dielectric constants.

There are several formulas used to explain the relationships between the dielectric constant, capacitance, water absorption and coating failure parameters. The parallel plate model formula (1) [41] describe show, when an electrolyte solution with a large dielectric constant penetrates into the coating, the dielectric constant K of the coating will increase and, when the coating area (A) and thickness (d) are constant, the corresponding capacitance (C) of the coating will also increase. According to formula (2) [42], it can be known that the foaming rate or porosity parameter F of the coating will increase. This parameter corresponds to the microscopic foaming and micropore production of the coating, which reduces the corrosion resistance of the coating. As for the water absorption rate of the coating, we can refer to the formula (3) [42]: when the water absorption of the coating ($Xv\%$) is low, the coating capacitance only changes a little with time. That is to say, C(0) and C(t) are approximately equal.

$$C = K\varepsilon_0 \frac{A}{d} \tag{1}$$

$$C = C^0 F \tag{2}$$

$$X_V\% = 100 \times \log[C(t)/C(0)]/\log(80) \tag{3}$$

C^0: coating capacitance per unit area; $Xv\%$: the water absorption of the coating; $C(0)$: Coating starting capacitance; $C(t)$: Coating capacitance at time t.

Some researchers also reported that the higher cross-link density of the coating could increase electrochemical corrosion [16,43,44]. P. Thirukumaran synthesized bio-based benzoxazines 6-allyl-8-methoxy-3-octadecyl-3, 4-dihydro-2H-benzoxazin (S-Bz) and 6-allyl-3 –(furan-2-ylmethl)-8-methoxy-3, 4-dihydro-2H-benzoxazine (F-Bz) [44]. It was found that the corresponding polymer PS-Bz has good flexibility and that PF-Bz has good crosslink density, although their corrosion resistance was not reported.

Naturally, we are motivated to study the anti-corrosion of bio-based benzoxazine coating with low dielectric constant, low water absorption and high cross-link density organic resins in order to improve upon corrosion protection. In this work, we expanded our previous research and synthesized a new bio-based benzoxazine resin (Scheme 1), D-Bz (Dehydroabietylamine benzoxazine monomer). Since the PD-Bz (Dehydroabietylamine polybenzoxazine) has a low dielectric constant and more stable electrochemical corrosion resistance, we studied the copolymer of D-Bz with S-Bz and F-Bz in order to achieve higher electrochemical corrosion protection efficiency. The thermal curing process, thermal stability, crosslink density, contact angle, water absorption, dielectric properties and electrochemical corrosion resistance of the coating was investigated.

2. Experimental

2.1. Materials

Dehydroabietylamine (90%), furfurylamine (99%), octadecylamine (99%), sodium chloride (99.5%), sodium bicarbonate (AR grade), sodium hydroxide (AR grade), eugenol (99%), paraformaldehyde (AR grade), dioxane (AR grade), tetrahydrofuran (AR grade), acetic acid (AR grade), ethanol (AR grade) and anhydrous acetone (AR grade) were

purchased from Sigma-Aldrich. Chemicals and solvents were used as-received without further purification. The Q235 carbon steel (10 mm × 10 mm × 0.2 mm) electrodes were rinsed by ultrasonication in anhydrous acetone and anhydrous ethanol for cleaning the surface contaminants. After that, the Q235 were polished using 400, 800 and 1500-grit sand papers.

2.2. Synthesis of monomers

2.2.1. Synthesis of D-Bz

D-Bz was prepared by the fowling procedure: under condensed reflux conditions, eugenol (30 mmol, 4.92 g), dehydroabietylamine (30 mmol, 9.50 g) and paraformaldehyde (60 mmol, 1.8 g) were placed in a 500 mL round-bottomed flask (Scheme 1). Then 200 mL of dioxane was added as the solvent. The mixture was stirred at 70 °C until it was completely dissolved, and then the mixture was heated to 85 °C and maintained at this temperature for 12 h. After cooling to room temperature, the crude product was concentrated under reduced pressure to remove dioxane, and the residual solid washed several times with 95 °C 1% aqueous NaHCO₃ to remove unreacted eugenol. The product was purified by recrystallizing in ethanol to remove dehydroabietylamine and by products. The resulting powdery brown solid was dried at 65 °C in a vacuum oven. The yield was 77%, and the melting point was 97 °C. FTIR (KBr, cm⁻¹) is shown in Fig. S1: 2930 (C—H), 2865 (C—H), 1233 (C—O—C), 1158 (C—N—C), 1092 (C—O—C), 938 (C—H). ¹H NMR (400 MHz, CDCl₃, δ, ppm) is shown in Fig. S2: 7.2–6.2 (Ar—H), 3.8 (—OCH₃), 5.9, 5.0 and 3.2 (—CH₂—CH=CH), 4.8 (O—CH₂—N), 3.7 (Ar—CH₂—N). Mass spectrometry (MS) (m/z) is 473.2 as shown in Fig. S3. (The theoretical molecular weight of D-Bz is 473 g/mol).

2.2.2. Synthesis of S-Bz

S-Bz (6-allyl-8-methoxy-3-octadecyl-3, 4-dihydro-2H-benzoxazin) was prepared based on already reported method [43,44]. The reaction process is shown in Scheme 1. The yield was 87%, and the melting point was 50 °C. FT-IR (KBr, cm⁻¹) is shown in Fig. S1: 2930 (C—H), 2865 (C—H), 1230 and 1092 (C—O—C), 1154 (C—N—C), 944 (C—H). ¹H NMR (400 MHz, CDCl₃, δ, ppm) is shown in Fig. S4: 3.8 (—OCH₃), 3.2, 5.9 and 5.0 (—CH₂—CH=CH), 4.8 (O—CH₂—N), 3.9 (Ar—CH₂—N).

2.2.3. Synthesis of F-Bz

F-Bz (6-allyl-3 –(furan-2-ylmethl)-8-methoxy-3, 4-dihydro-2H-benzoxazine) was prepared based on already reported method [43,44]. The reaction process is shown in Scheme 1. The yield was 93%, and the melting point was 75 °C. FT-IR (KBr, cm⁻¹) is shown in Fig. S1: 2930 (C—H), 2865 (C—H), 1589, 1003 and 733 (vibrations of the furan ring), 1233 and 1095 (C—O—C), 1146 (C—N—C), 1092 (C—O—C), 943 (C—H). ¹H NMR (400 MHz, CDCl₃, δ, ppm) is shown in Fig. S5: 6.63–6.45 (Ar—H), 3.8 (—OCH3), 5.9, 5.0 and 3.2 (—CH₂—CH=CH), 7.3, 6.8–6.2 (Hydrogen proton on furan ring), 4.8(O—CH₂—N), 4.0 (Ar—CH₂—N).

2.3. Preparation of corresponding polybenzoxazines and copolymers

The three benzoxazine monomers, S-Bz, D-Bz, and F-Bz, were mixed according to a certain molar ratio (Table 1), dissolved in tetrahydrofuran (THF) and the solution poured into ceramic models. Then, the ceramic models were placed into a vacuum drying oven at 80 °C for 24 h to remove the solvent. After that, they were cured in a tube furnace and the steps were as follows: 100 °C (1 h), 150 °C (1 h), 180 °C (2 h), 200 °C (2 h), and 230 °C (1 h). Thereafter, samples were cooled to room temperature and the resulting polymers were named PSDF-Bz (Table 1).

2.4. Characterization

FTIR spectra were measured with a Bruker Vector 22 FTIR analyzer. All samples were finely ground with KBr powder and pressed into a thin
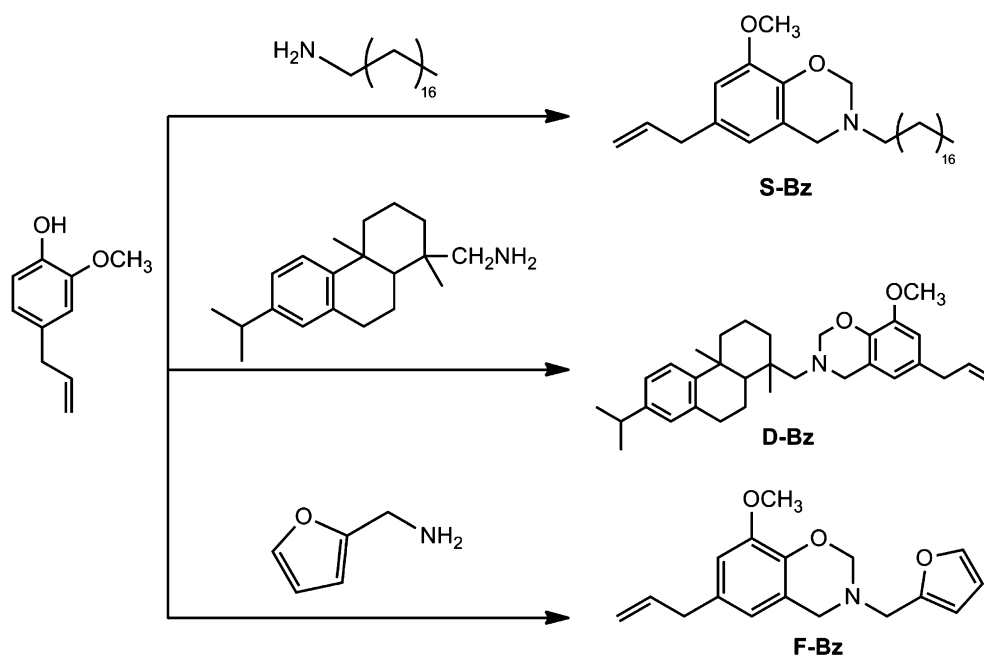
Scheme 1. Structure of bio-based benzoxazine monomers (D-Bz, S-Bz, F-Bz).

Table 1
The name of the cured resin and its monomer ratio.

Monomer	S-Bz	D-Bz	F-Bz	Corresponding polymer
SDF-Bz(10/0/0)	10	0	0	PSDF-Bz(10/0/0)
SDF-Bz(0/10/0)	0	10	0	PSDF-Bz(0/10/0)
SDF-Bz(0/0/10)	0	0	10	PSDF-Bz(0/0/10)
SDF-Bz(4/6/0)	4	6	0	PSDF-Bz(4/6/0)
SDF-Bz(3/6/1)	3	6	1	PSDF-Bz(3/6/1)
SDF-Bz(2/6/2)	2	6	2	PSDF-Bz(2/6/2)
SDF-Bz(1/6/3)	1	6	3	PSDF-Bz(1/6/3)
SDF-Bz(0/6/4)	0	6	4	PSDF-Bz(0/6/4)

Table
2. DSC data of SDF-Bzs.

Name	T_m (°C)	T_{onset} (°C)	T_{max} (°C)	Processiing windows (°C)
SDF-Bz(10/0/0)	50	193	221	143
SDF-Bz(0/10/0)	97	198	226	101
SDF-Bz(0/0/10)	75	169	210	94
SDF-Bz(4/6/0)	54/97	194	223	97
SDF-Bz(3/6/1)	53/74/97	187	219	90
SDF-Bz(3/6/2)	53/74/97	182	215	85
SDF-Bz(1/6/3)	53/74/97	183	213	86
SDF-Bz(0/6/4)	74/97	177	212	80

disk. ^{1}H NMR spectra were recorded with ^{1}H NMR spectrometer (Bruker, 400 MHz) using CDCl$_3$ as the solvent and TMS as the internal standard. DSC was carried out on an Instruments DSC Model 2920. Both samples were heated at a rate of 10 °C/min under nitrogen flow of 50 mL/min, and an indium standard was used for calibration. The glass transition temperature (Tg) of polybenzoxazine was studied by DSC. TGA was carried out on a TA Instrument Model 2050 with a heating rate of 10 °C/min under nitrogen flow of 40 mL/min. The dielectric properties of polybenzoxazines were analyzed with a Concept 40 Broadband dielectric analyzer at 25 °C. The crosslinking density of corresponding polybenzoxazines was analyzed with IIC XLDS-15 analyzer at room temperature. Tafel, electrochemical impedance spectroscopy (EIS) and OPCT curves and Tafel plots were studied with an Electrochemical Workstation CHI 760E. Q235 low-carbon steels (1 cm × 1 cm × 0.2 cm) were washed with acetone twice before being used. All samples were immersed in 3.5% sodium chloride saline for 7 days before electrochemical tests. The morphology of the coated and uncoated steels were observed by SEM.

3. Results and discussion

3.1. Curing behavior of SDF-Bz

The polymerization behavior of the SDF-Bz resins was studied by DSC (Fig. S6). The bulky amine moiety does not degrade during the cure [45,46] and the relevant parameters of the monomer curing process are shown in Table 2. The endothermic peaks at 50, 97 and 75 °C

are assigned to the melting points of S-Bz, D-Bz and F-Bz, respectively. The exothermic peaks demonstrate the ring-opening polymerization of oxazine rings. The onset ring-opening temperatures of S-Bz and D-Bz are 193 °C and 198 °C, while the value for F-Bz is 169 °C due to the electrophilic substitution reaction of furan ring [47].

Fig. S6b displays the curing process of the copolymer. The relevant data are summarized in Table 2. As the content of F-Bz increases in the copolymer SDF-Bz, the curing exothermic peak gradually shifts to a lower temperature.

3.2. Thermal properties of PSDF-Bz

Figs. S7 and S8 display the thermal properties of PSDF-Bz, and Table 3 summarizes the data. The Tg of PSDF-Bz(0/0/10) has the highest temperature of 148 °C due to the furan ring in PSDF-Bz(0/0/10) which increases crosslink density [46]. In addition, hydrogen bonds formed by oxygen atoms in the furan ring also increase the Tg [48]. PSDF-Bz(10/0/0) contains a long alkyl chain and the molecule is relatively soft, which makes the Tg of PSDF-Bz(10/0/0) lower. As the content of F-Bz increases in the copolymer, the Tg tends to increase. The Tg of copolymers were also calculated by the FOX formula, as shown in formula (4) and it was found that the Tg_{FOX} were close to the experimental dates [49]. Moreover, only one Tg is found in all copolymers, which indirectly reflects the good compatibility of the three resins in the copolymer.

$$\frac{1}{T_g} = \frac{w_1}{T_{g_1}} + ... + \frac{W_n}{T_{g_n}}$$

(4)

Table 3
Thermal properties and crosslink density of PSDF-Bzs.

Sample	T_5 (°C)	T_{10} (°C)	CY (%)	LOI values	T_g (°C)	$T_{g_{FOX}}$ (°C)	Crosslink density (*E^{-4} mol/ml)
PSDF-Bz (10/0/0)	316	346	24	27.1	101	–	3.617
PSDF-Bz (0/10/0)	341	378	38	32.7	135	–	4.762
PSDF-Bz (0/0/10)	375	405	54	39.1	148	–	5.585
PSDF-Bz (4/6/0)	320	358	32.4	30.46	118	120	4.88
PSDF-Bz (3/6/1)	327	363	35	31.5	123	125	5.038
PSDF-Bz (2/6/2)	348	382	36	31.9	130	130	5.165
PSDF-Bz (1/6/3)	357	388	38	32.7	133	135	5.289
PSDF-Bz (0/6/4)	368	394	41	33.9	137	139	5.433

$W_1...W_n$ are the mass percentage of each type of monomers, $T_{g1}...T_{gn}$ are the glass transition temperature of each type of monomer homopolymers (the unit is K).

The TGA curves of PSDF-Bzs show that the onset weight-loss of the polymers and copolymers are beyond 300 °C (Fig. S8); it is associated with the degradation at the Mannich bridge. The temperatures of 5% weight-loss (T_5) of all copolymers are higher than 300 °C, which means they all have good thermal stability.

The Limit Oxygen Index (LOI) value of the coating is also an important indicator of its flame retardancy [50]. LOI values were calculated from the TGA data using the Van Krevelan and Hofytzerequations [50]. The formula (5) is as follows:

$$LOI = 17.5 + 0.4CY \qquad (5)$$

Table 3 summarizes the LOI of homopolymers and copolymers. CY is Carbon Yield. It can be seen that the LOI value increases with the increase in F-Bz content. The LOI value of all copolymer resins exceeds 30. It is known that most bio-based benzoxazine resins have poor thermal properties. This result indicates that the PSDF-Bz(0/0/10) may have greater applications than ordinary bio-based benzoxazine.

3.3. Dielectric properties of polymer and copolymer coatings

Fig. 1 shows the dielectric constant and dielectric loss of PSDF-Bzs. It has been found that the dielectric constants of all copolymers are lower than 2.9 when the frequency is greater than 10^3 Hz, moreover, they have low dielectric loss. They are much lower than that of other PBzs, where the dielectric constant is usually in the range of 2.5–4 [51,52]. It is expected that this excellent dielectric property means the copolymers may have high molar volumes and may have a good effect on the corrosion resistance of the copolymer, according to formula (1) [41].

3.4. Static water contact angle (CA)

In order to investigate the surface hydrophobicity, CA measurements were performed on bare carbon steel and various coated samples before exposure in a corrosive medium. As shown in Fig. 2, with the absence of a protective coating, Q235 steel could be readily attacked by corrosive species due to its hydrophilic surface (CA = 87.5°) and primordial battery system. The PSDF-Bz(10/0/0) coating shows a higher CA of 109.33°, caused by the hydrogen bonds and long aliphatic groups in the PSDF-Bz, which results in the low SFE energy of PSDF-Bz [30,53]. The crosslink network of PSDF-Bz can also diminish the permeability of water to the metallic substrate [54,55].

It has also been shown that, as the content of F-Bz increases, the CA values decrease since the PF-Bz has more hydroxyl groups which enable the membrane surface to bond with more water molecules [16]. Whilst not as good for anti-corrosion, hydroxyl groups also contribute to the interfacial adhesion between Q235 and resins, which can prevent the permeation of water [56,57].

3.5. Water absorption behavior

The water absorption behavior of the PSDF-Bz coatings were studied in 3.5% NaCl aqueous solution for 20 days. The results are shown in Fig. 3. On the 10th day, the water absorption of all the samples reached a saturated state; the saturated water absorption rates were less than 2%. In addition, the water absorptions of most copolymer coatings were lower than of a homopolymer. Further, it was found that the water absorbability of the resin slightly changed with the composition of the copolymer. This result reflects the synergistic effect of resins in the copolymer [58]. An increase in the furan ring concentration improves the crosslink density of the coating [59], which could reduce the free space. Besides this effect, the nature of the material also affects the water absorption of the material and the long alkyl chain imparts a low surface energy to the PBz coatings, making it difficult for water molecules to contact the surface of the material. It was found that copolymer PSDF-Bz(3/6/1) shows the lowest water absorption rate of only 0.988% after 20 days. Copolymer PSDF-Bz(1/6/3) and PSDF-Bz(2/6/2) also have low water absorption.
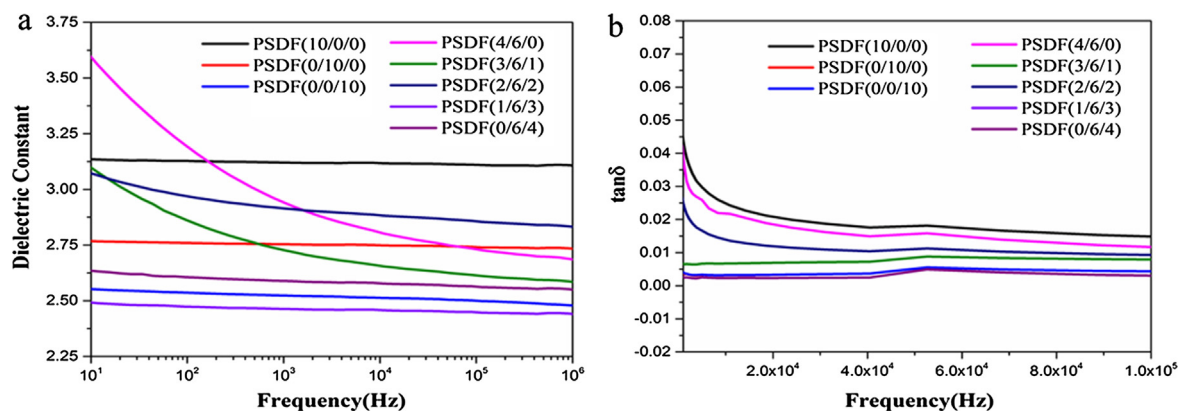

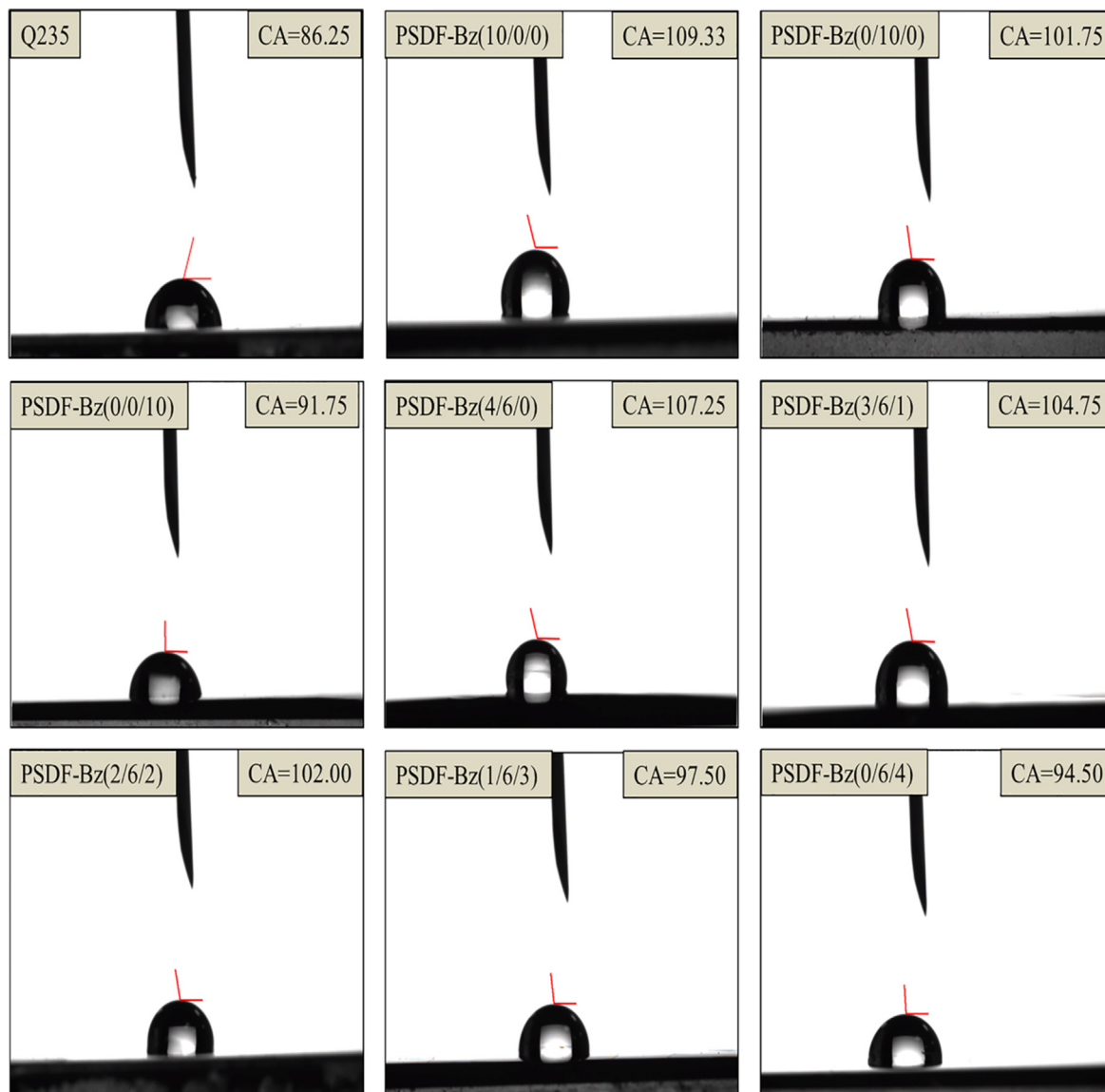**Fig. 1.** Dielectric property of PSDF-Bzs (a) Dielectric Constant (b) Dielectric Loss.

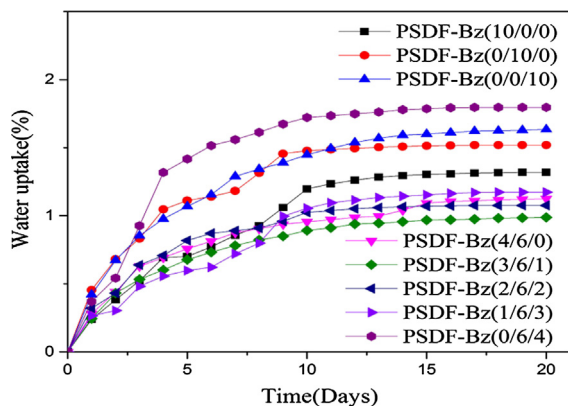**Fig. 2.** Static water contact angles of Q235 and PBz coatings.

Fig. 3. Water absorption curves of PSDF-Bz at 25 °C.

3.6. Open circuit potential time (OCPT) characterization

The corrosion resistant properties were observed in 3.5 wt% NaCl aqueous solutions for coated and uncoated Q235 steel using an electrochemical work station. The OCPT, Tafel curve and EIS spectra were evaluated to study the corrosion resistance of PSDF-Bz coatings. The open circuit voltages (E_{ocp}), recorded for both coated and uncoated Q235 steel, were plotted as a function of immersion time. Compared with Q235 carbon steel without the PSDF-Bz coating, the E_{ocp} value of coated Q235 carbon steel increased from −1.019 V to −0.7014 V after 100 min of immersion time. It can be seen from Fig. 4 that, among the three homopolybenzoxazine coatings, the E_{ocp} of PSDF-Bz (0/10/0) is highest after 3500 s immersion and shows only comparatively small changes over time, suggesting that the PSDF-Bz (0/10/0) has excellent corrosion resistance [60,61]. Since E_{ocp} is related to CA and water absorption, despite the initial E_{ocp} of PSDF-Bz (0/0/10) being high, immersion in a 3.5% NaCl aqueous solution for 6000 s reduces E_{ocp} to −0.7581 V (due to its high water absorption and poor hydrophobicity). The corresponding microscopic interpretation is that water molecules can easily enter the metal surface through pores in the coating/substrate, resulting in a decline in E_{ocp} data for later testing. Although PSDF-Bz(10/0/0) has good hydrophobicity (CA = 109.33°) and low water absorption (1.319%), its E_{ocp} is still lower than the other two samples. The reason for this phenomenon may be that the long alkyl chain imparts a lower surface free energy to the material, reducing its affinity to the metal matrix; therefore, the adhesion between the metal and the coating of the material is not strong.
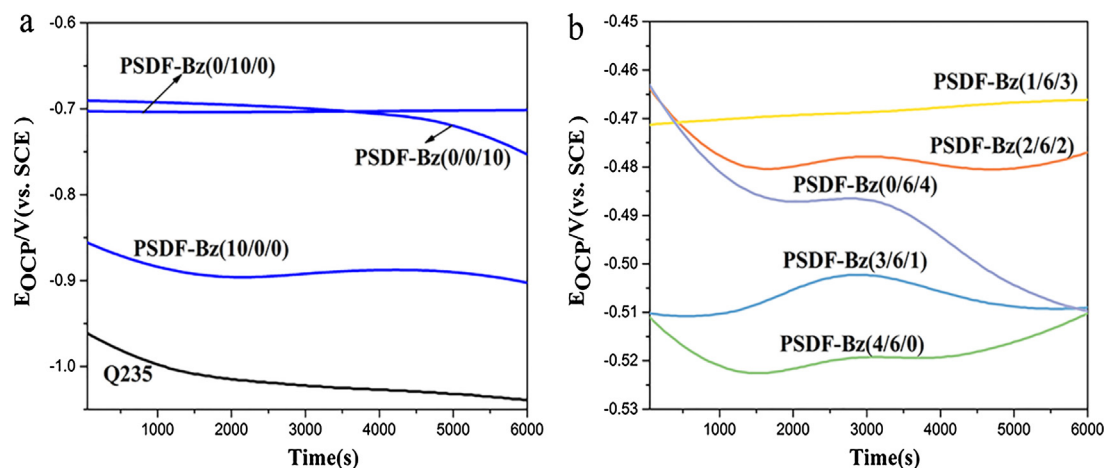
Fig. 4. The OCPT values of coated and uncoated Q235 steels.

As shown in Fig. 4b, copolymer coated Q235 steel has more positive E_ocp values compared to uncoated Q235 steel or homopolymer-coated Q235 steel, even after 6000 s exposure to 3.5% NaCl aqueous solution. The E_ocp of PSDF-Bz (0/6/4) with higher water absorption and lower hydrophobicity decreased rapidly with time. Samples with lower water absorption, such as PSDF-Bz (1/6/3) and PSDF-Bz (2/6/2), show a larger E_ocp, while PSDF-Bz (3/6/1) and PSDF-Bz (4/6/0), which have better hydrophobicity and low water absorption rates, have a more negative E_ocp. A possible reason for this effect is that the dielectric coefficient results in an increase in tantalum capacitance and a more negative E_ocp while forming the electrolytic cell. The PSDF-Bz(1/6/3) coated carbon steel shows high initial and lowest Eocp (−0.4713 V to −0.4661 V) values, which means it may have higher corrosion resistance.

3.7. Tafel characterization

The Tafel plots obtained by immersing the samples in 3.5% NaCl aqueous solution are shown in Fig. 5 and Table 4. All electrochemical tests are averages of 10 samples except extreme data. Corrosion potential (E_{corr}) and corrosion current (I_{corr}) were obtained using the extrapolation method [62,63]. Amore negative E_{corr} and larger I_{corr} usually correspond to a faster corrosion rate while a more positive E_{corr} and smaller I_{corr} mean a slower corrosion process [64]. The protection efficiencies (E%) are calculated using formula (6) [65,66]:

$$E(\%) = [(I_{corr} - I_{corr}(c))/I_{corr}]*100 \qquad (6)$$

$E(\%)$ is the metal protection efficiency. I_{corr} and $I_{corr}(c)$ are the corrosion current values in the absence and presence of the coatings, respectively. The corrosion rate and protection efficiency could be calculated from E_{corr} and I_{corr} for quantitative evaluation of the anticorrosion performance (Table 4). In the case of bare low carbon steel, the E_{corr} is −0.573 V, which is improved to −0.497 V (PSDF-Bz (10/0/0)), −0.371 V (PSDF-Bz (0/10/0)) and −0.325 V (PSDF-Bz (0/0/10)) when coated with the cured homopolymer of benzoxazine. Moreover, the current of anodic polarization curve of the PSDF-Bz samples showed a significant decrease, which means that the anodic dissolution process of the metals were delayed due to the benzoxazine coatings.

It can be seen that the PSDF-Bz(3/6/1), PSDF-Bz(2/6/2) and PSDF-Bz(1/6/3) have the highest corrosion protection efficiency. The corresponding corrosion resistance E% values are 98.87%, 99.23% and 99.74%, respectively. These data are higher than for homopolymers (PSDF-Bz(10/0/0), PSDF-Bz(0/10/0) and PSDF-Bz (0/0/10)) due to the synergistic effect. This result reflects the synergistic effect of the three components. PSDF-Bz (3/6/1), PSDF-Bz (2/6/2) and PSDF-Bz (1/6/3) coatings also have low water absorption and excellent dielectric properties resulting in a small portion of water molecules entering the polymer network, which hindered the closed circuit of the metal substrate and the power supply electrode [16,67,68]. Besides low water absorption, PSDF-Bz (1/6/3) has a lower dielectric constant, that is to say, the number of microcapacitors per unit volume of the coating is lower and the resulting interface polarization is weaker. Logically, the PSDF-Bz (1/6/3) coating has the lowest electrochemical corrosion rate
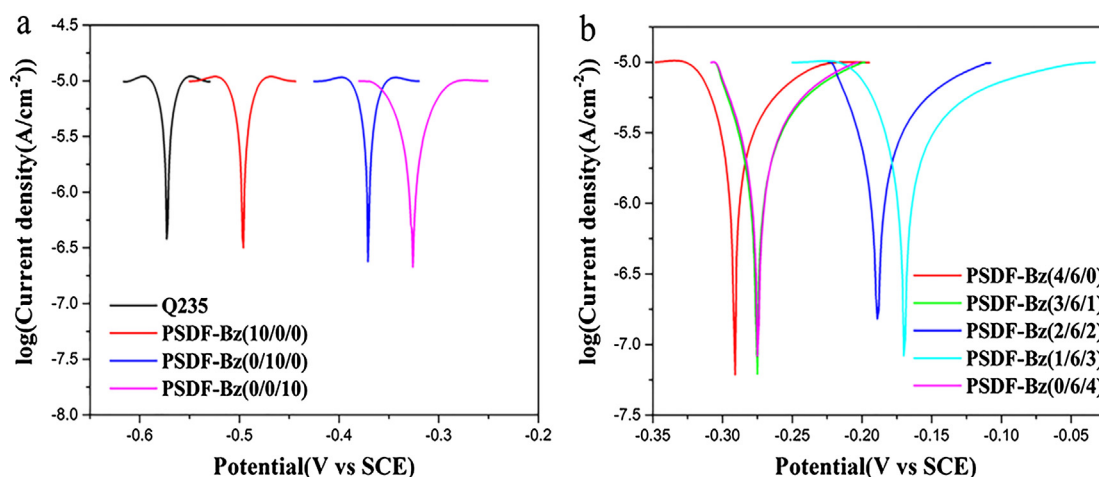

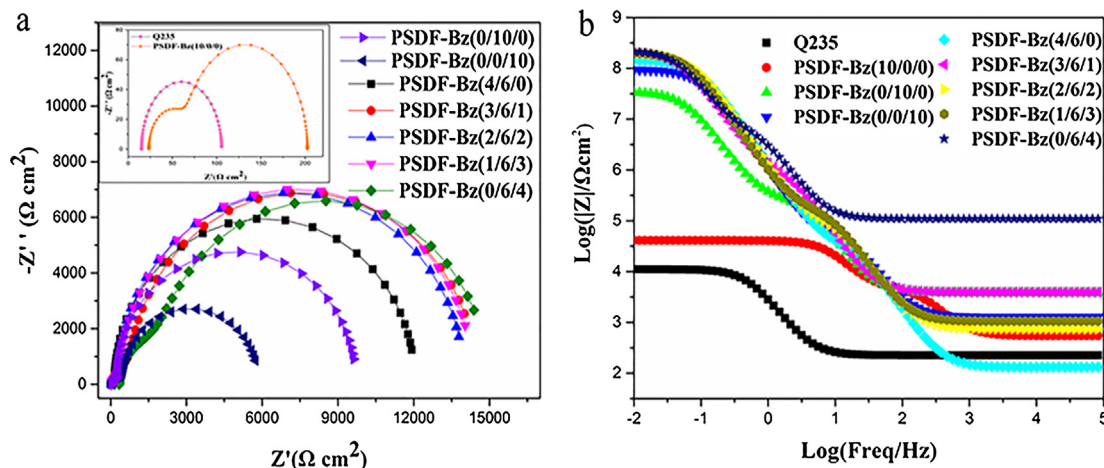**Fig. 5.** The Tafel curves of coated and uncoated Q235 steels.

Fig. 6. (a) Nyquist plots of coated and uncoated Q235 steels; (b) Bode plots of coated and uncoated Q235 steels.

Table 4
Result of electrochemical corrosion measurement in 3.5% NaCl solution.

| Sample	E_{corr} (V)	I_{corr} (µA/cm^2)	Corrosion rate (mm/year)	Protection efficiency E (%)
Bare metal	− 0.573	11.600	$5.298 * 10^{-2}$	–
PSDF-Bz (10/0/0)	− 0.497	6.472	$2.956 * 10^{-2}$	44.21
PSDF-Bz (0/10/0)	− 0.371	1.899	$8.733 * 10^{-3}$	83.63
PSDF-Bz (0/0/10)	− 0.325	1.304	$5.954 * 10^{-3}$	88.96
PSDF-Bz (4/6/0)	− 0.291	0.807	$3.689 * 10^{-3}$	93.04
PSDF-Bz (3/6/1)	− 0.275	0.131	$5.984 * 10^{-5}$	98.87
PSDF-Bz (2/6/2)	− 0.189	0.089	$4.097 * 10^{-5}$	99.23
PSDF-Bz (1/6/3)	− 0.170	0.030	$1.402 * 10^{-5}$	99.74
PSDF-Bz (0/6/4)	− 0.278	0.275	$1.255 * 10^{-4}$	97.63
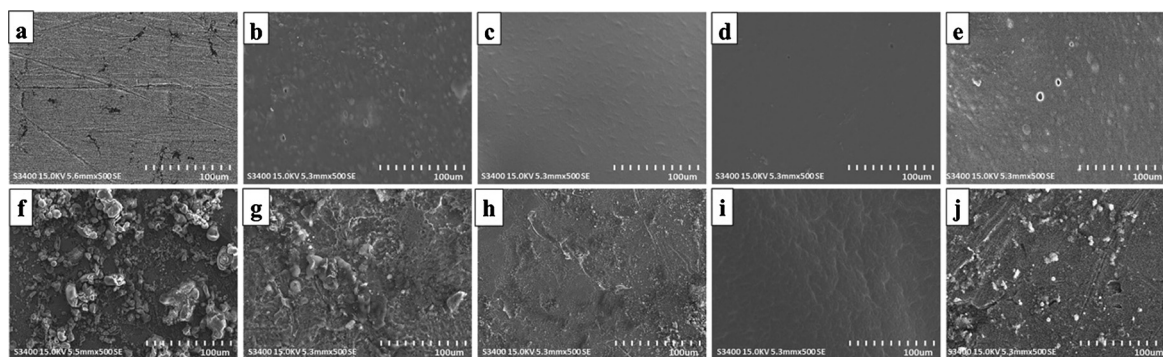
Fig. 7. SEM images of (a) Bare steel (b) PSDF-Bz(0/10/0) (c) PSDF-Bz(3/6/1) (d) PSDF-Bz(1/6/3) (e) PSDF-Bz(0/6/4) before immersion and after 7 days immersion (f), (g), (h), (i), (j).

and the highest corrosion resistance efficiency (E% = 99.74%).

3.8. Electrochemical impedance spectra characterization

Generally, electrochemical impedance spectra (EIS) and SEM images (Fig. 7) of the morphology before and after corrosion are used to further evaluate and compare the barrier and the anticorrosion ability of composite coatings in a corrosive medium such as 3.5% NaCl solution [55,69]. The EIS results were fitted by Z view software based on different equivalent circuit models to quantitatively assess the performance of these coatings.

The relationship between the dielectric constant, water absorption and EIS results can be analyzed according to formula (3). During the process of corrosion of a polymer-coated metal, we refer to the time when the water does not reach the coating/substrate interface. As shown in formula (3), at this stage, water molecules continuously enter the coating, and the water absorption of the polymer coating (X_V%)

increases, resulting in an increase in $C(t)$. The penetration of the electrolyte solution into the coating will reach saturation after a certain period of time, after which the coating capacitance (C_c) will no longer increase significantly due to changes in the dielectric constant of the coating [42]; however, as the electrolyte solution penetrates to the interface of the coating/substrate and forms a corrosion-reactive microbattery in the interfacial zone, the measured impedance spectrum will have two time constants. The time that the impedance spectrum appears two time constants, while the surface of the coating do not yet formed macroscopic pores, is called the mid-soaking period.

The evaluation of the performance of the coating by the EIS measurement in the middle of the immersion is extremely important because the results of the impedance measurements are extremely sensitive to a change in information on coating/substrate interface structure. Furthermore, the Nyquist plots of uncoated mild steel Q235 were fitted using an equivalent circuit of R(CR), as presented in Fig. 8a, and then coated mild steel Q235 in the mid-soaking period of the immersion
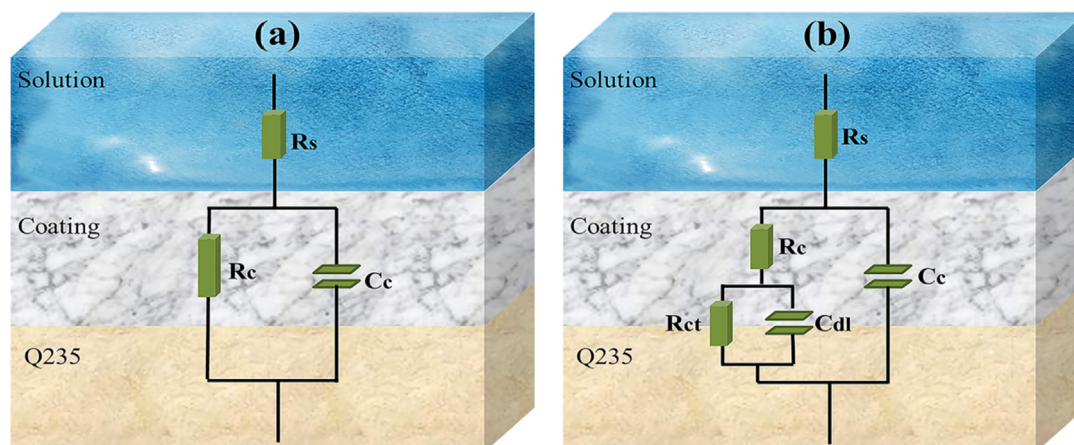
Fig. 8. The proposed circuit model for (a) uncoated Q235 steel and (b) coated Q235 steels.

Table 5
Anticorrosion properties of Q235 and PSDF-Bz coatings.

Sample	R_s (Ω cm^2)	$C_c * 10^{-5}$ (F cm^{-2})	R_c (Ω cm^2)	$C_{dl} * 10^{-4}$ (F cm^{-2})	R_{ct} (Ω cm^2)
Q235	10.56	–	–	31.40	90.52
PSDF-Bz(10/0/0)	23.4	1.44	52.74	1.270	126.3
PSDF-Bz(0/10/0)	61.5	7.951	556.9	4.125	5251
PSDF-Bz(0/0/10)	35.8	4.035	261.9	4.45	9411
PSDF-Bz(4/6/0)	11.5	3.91	249	1.03	1118
PSDF-Bz(3/6/1)	62.7	7.01	1431	1.61	13,000
PSDF-Bz(2/6/2)	27.21	4.55	4042	1.061	13,570
PSDF-Bz(1/6/3)	32.58	4.464	5315	1.330	13,800
PSDF-Bz(0/6/4)	33.12	8.064	3280	2.11	11,330

were fitted using an equivalent circuit of R(CR)(CR), as presented in Fig. 8b. In the second model, the electrolyte solution penetrates into the coating/substrate interface through the microspores on the surface of the coating and the foaming of the interface region is local, corresponding to the microspores.

Considering the equivalent circuit model proposed for PSDF-Bz coatings, R_c (coating resistance) and C_c (coating capacitance) are related to electrolyte/coating interface; R_{ct} and C_{dl} are also related to the charge transfer reactions at the electrolyte/substrate interface [70]. The corresponding parameters derived from the two models are summarized in Table 5. All electrochemical tests are averages of 10 samples except extreme data.

As shown by Nyquist polt (Fig. 6), The PSDF-Bz(1/6/3) coated steel sample shows the maximum diameter of the semicircle; the value of R_c is found to be 5.315 Ω cm^2. The value of R_{ct} is the transfer resistance between the electrolyte and the substrate. In general, the magnitude of the R_{ct} value reflects the difficulty of charge transfer in the metal matrix. The larger the value of R_{ct}, the better the corrosion resistance of the coating has. As shown in Table 5, the R_c value of the copolymerized benzoxazine resin is 1–2 orders of magnitude higher than the coating resistance of the homopolybenzoxazine resin. A similar phenomenon is found in the R_{ct}.

This phenomenon is attributed to the synergistic effect of each component of the copolymer resin. The long alkyl chain in PSDF-Bz(10/0/0) imparts excellent hydrophobicity to the coating and PSDF-Bz(0/10/0) improves steady corrosion resistance. Furthermore, the low dielectric constant inherent with PSDF-Bz(0/0/10) and the high crosslink density of the furan ring promotes cross-linking. From Table 4 and Fig. 8, it can be seen that, with a decrease in the dielectric constant of the copolymer, the interfacial polarization will decrease during electrochemical corrosion. Therefore, PSDF-Bz (1/6/3) displays the best synergistic effects with a low dielectric constant, low water absorption, high coating capacitance and coating resistance, which all result in the best anticorrosion properties among the PSDF-Bz copolymers.

4. Conclusions

In this study, a novel low dielectric and fully bio-based benzoxazine D-Bz was synthesized and copolymerized with S-Bz and F-Bz. It was found that, when the ratio of S-Bz:D-Bz:F-Bz was 1:6:3, the copolymer shows good synergistic effects. It is found that PSDF-Bz(1/6/3) has both a low curing temperature (183 °C) and a high residual carbon ratio (38%). Dielectric characterization, CA and water absorption tests show that PSDF-Bz(1/6/3) has excellent dielectric stability (2.47 at 1000 Hz), and low hydrophilicity (CA 97.5°) and water absorption (0.98%). In conclusion, PSDF-Bz(1/6/3)'s electrochemical corrosion resistance tests show excellent performance values, with corrosion protection efficiency up to 99.73%.

Appendix A. Supplementary material

Supplementary data to this article can be found online at https://doi.org/10.1016/j.eurpolymj.2019.07.020.

References

[1] A. Mohammadi, M. Barikani, A.H. Doctorsafaei, A.P. Isfahani, E. Shams, B. Ghalei, Aqueous dispersion of polyurethane nanocomposites based on calix [4] arenes modified graphene oxide nanosheets: Preparation, characterization, and anti-

corrosion properties, Chem. Eng. J. 349 (2018) 466–480.

[2] A. Seongpil, W.L. Min, L.Y. Alexander, S.Y. Sam, A review on corrosion-protective extrinsic self-healing: comparison of microcapsule-based systems and those based on core-shell vascular networks, Chem. Eng. J. 344 (2018) 206–220.

[3] G.S. Morteza, S. Mohammadreza, R. Bahram, Fabricating an epoxy composite coating with enhanced corrosion resistance through impregnation of functionalized graphene oxide-co-montmorillonite nanoplateletp, Corros. 129 (2017) 38–53.

[4] Y.Y. Qian, Y.X. Li, S. Jungwirth, N. Seely, Y. Fang, X.M. Shi, The application of anti-corrosion coating for preserving the value of equipment asset in chloride-laden environments: a review, Int. J. Electrochem. Sci. 10 (2015) 10756–10780.

[5] F. Khelife, S. Ershov, M. Druart, Y. Habibi, D. Chicot, A multilayer coating with optimized properties for corrosion protection of Al, J. Mater. Chem. 3 (2015) 15977.

[6] A. Renaud, M. Poorteman, J. Escobar, L. Dumas, Y. Paint, P. Dubois, M.G. Olivier, A new corrosion protection approach for aeronautical applications combining a Phenol-paraPhenyleneDiAmine benzoxazine resin applied on sulfo-tartaric ano-dized aluminum, Prog. Org. Coat 112 (2017) 278–287.

[7] B. Nikravesh, B. Ramezanzadeh, A.A. Sarabi, S.M. Kasiriha, Evaluation of the cor-rosion resistance of an epoxy-polyamide coating containing different ratios of mi-caceous iron oxide/Al pigments, Corros. Sci. 53 (4) (2011) 1592–1603.

[8] S.S. Jia, X.H. Lu, S. Luo, Y. Qing, N. Yan, Y.Q. Wu, Efficiently texturing hierarchical epoxy layer for smart superhydrophobic surfaces with excellent durability and ex-ceptional stability exposed to fire, Chem. Eng. J. 348 (2018) 212–223.

[9] Z.J. Thompson, M.A. Hillmyer, J. Liu, H.J. Sue, M. Dettloff, F.S. Bates, Block co-polymer toughened epoxy: role of cross-link density, Macros 42 (7) (2009) 2333–2335.

[10] B. Ramezanzadeh, G. Bahlakeh, M. Ramezanzadeh, Polyaniline-cerium oxide (PAni-CeO2) coated graphene oxide for enhancement of epoxy coating corrosion protec-tion performance on mild steel, Corros. Sci. 137 (2018) 111–126.

[11] B. Grgur, M. Gvozdenović, V. Mišković-Stanković, Corrosion behavior and thermal stability of electrodeposited PANI/epoxy coating system on mild steel in sodium chloride solution, Prog. Org. Coat. 56 (2) (2006) 214–219.

[12] C.L. Zhou, J.P. Lin, X. Lu, Z. Xin, Enhanced corrosion resistance of polybenzoxazine coatings by epoxy incorporation, RSC Adv. 6 (34) (2016) 28428–28434.

[13] P. Campaner, D. D'Amico, L. Longo, C. Stifani, A. Tarzia, Cardanol-based novolac resins as curing agents of epoxy resins, J. Appl. Polym. Sci. 114 (6) (2010) 3585–3591.

[14] S.W. Choi, S. Ohba, Z. Brunovska, K. Hemvichian, H. Ishida, Synthesis, character-ization and thermal degradation of functional benzoxazine monomers and polymers containing phenylphosphine oxide, Polym. Degrad. Stabil. 91 (5) (2006) 1166–1178.

[15] F.W. Holly, A.C. Cope, Condensation products of aldehydes and ketones with o-aminobenzyl alcohol and o-hydroxybenzylamine, J. Am. Chem. Soc. 66 (11) (1944) 1875–1879.

[16] G.A. Phalak, D.M. Patil, S.T. Mhaske, Synthesis and characterization of thermally curable Guaiacol based poly (benzoxazine –urethane) coating for corrosion pro-tection on mild steel, Eur. Polym. J. 88 (2016).

[17] H. Ishida, D.J. Allen, Physical and mechanical characterization of near-zero shrinkage polybenzoxazines, J. Polym. Sci. Pol. Phys. 34 (6) (2015) 1019–1030.

[18] A.Q. Dayo, B.C. Gao, J. Wang, W.B. Liu, M. Derradji, A.H. Shah, A.A. Babar, Natural hemp fiber reinforced polybenzoxazine composites: curing behavior, mechanical and thermal properties, Compos. Sci. Technol. 144 (2017).

[19] H.G. Dong, X. Zhong, X. Lu, Y. Lv, Effect of N-substituents on the surface char-acteristics and hydrogen bonding network of polybenzoxazines, Polymer 52 (4) (2011) 1092–1101.

[20] A.H. Telli, J. Hacaloglu, Effects of aromatic diboronic acid on thermal charateristics of polybenzoxazines based on phenol and aniline, Eur. Polym. J. 108 (2018) 182–190.

[21] L. Jin, T. Agag, H. Ishida, Bis(benzoxazine-maleimide) as a novel class of high performance resin: synthesis and properties, Eur. Polym. J 46 (2) (2010) 354–363.

[22] S. Saiev, L. Bonnaud, P. Dubois, D. Beljonne, R. Lazzaroni, Modeling the formation and thermomechanical properties of polybenzoxazine thermosets, Polym. Chem. 8 (2017) 5988.

[23] K. Zhang, Q. Zhuang, X. Liu, G. Yang, R. Cai, Z. Han, A new benzoxazine containing benzoxazole-functionalized polyhedral oligomeric silsesquioxane and the corre-sponding polybenzoxazine nanocomposites, Macros 46 (7) (2013) 2696–2704.

[24] K. Zhang, Z. Shang, C.J. Evans, L. Han, H. Ishida, S. Yang, Benzoxazine atropi-somers: intrinsic atropisomerization mechanism and conversion to high perfor-mance thermosets, Macros 51 (19) (2017) 7574–7585.

[25] S. Saiev, L. Bonnaud, L. Dumas, T. Zhang, P. Dubois, D. Beljonne, Do carbon na-notubes improve the thermomechanical properties of benzoxazine thermosets? ACS Appl. Mater. Interfaces 10 (2018) 26669–26677.

[26] A. Trejo-Machin, P. Verge, L. Puchot, R. Quintana, Phloretic acid as an alternative to the phenolation of aliphatic hydroxyls for the elaboration of polybenzoxazine, Green. Chem 19 (2017) 5065.

[27] L. Puchot, P. Verge, S. Peralta, Y. Habibi, C. Vancaeyzeele, Elaboration of bio-epoxy/benzoxazine interpenetrating polymer networks: a composition-to-mor-phology mapping, Polym. Chem. 9 (2018) 472.

[28] R.V. Lloyd, R. Jessica, H. Ishada, L. Diego, Development of fully biobased high-performance bis-benzoxazine under environmentally friendly conditions, ACS Sustain. Chem. 6 (2018) 5485–5494.

[29] C. Aydogan, B. Kiskan, S. Hacioglu, L. Toppare, Y. Yagci, Electrochemical manip-ulation of adhesion strength of polybenzoxazines on metal surfaces: from strong adhesion to dismantling, Rsc Adv. 4 (52) (2014) 27545–27551.

[30] S.C. Lin, C.S. Wu, J. Yeh, Y.L. Liu, Reaction mechanism and synergistic antic-orrosion property of reactive blends of maleimide-containing benzoxazine and

amine-capped aniline trimer, Polym. Chem. 5 (14) (2014) 4235–4244.

[31] E.B. Caldona, A.C. Leon, B. Pajarito, B.B. Pajarito, R.C. Advincula, Novel anti-cor-rosion coatings from rubber-modified polybenzoxazine-based polyaniline compo-sites, Appl. Surf. Sci. 422 (2017).

[32] M. Raicopol, B. Bălănucă, K. Sliozberg, B. Schluter, Vegetable oil-based poly-benzoxazine derivatives coatings on Zn–Mg–Al alloy coated steel, Corros. Sci. 100 (2015) 386–395.

[33] S. Li, C.X. Zhao, Y. Wang, L. Hui, Y.T. Li, Synthesis and electrochemical properties of electroactive aniline-dimer-based benzoxazines for advanced corrosion-resistant coatings, J. Mater. Sci. 53 (10) (2018) 7344–7356.

[34] M. Poorteman, A. Renaud, J. Escobar, L. Dumas, P. Dubois, Thermal curing of para-phenylenediamine benzoxazine for barriercoating applications on 1050 aluminum alloys, Prog. Org. Coat. 97 (2016) 99–109.

[35] A. Renaud, L. Bonnaud, L. Dumas, T. Zhang, P. Dubois, M.G. Olivier, A benzox-azine/substituted borazine composite coating: a new resin for improving the cor-rosion resistance of the pristine benzoxazine coating applied on aluminum, Eur. Polym. J. 109 (2018) 460–472.

[36] J. Escobar, M. Poorteman, L. Dumas, L. Bonnaud, P. Dubois, Thermal curing study of bisphenol a benzoxazine for barrier coatingapplications on 1050 aluminum alloy, Prog. Org. Coat. 79 (2015) 53–61.

[37] M.L. Salum, D. Iguchi, C.R. Arza, L. Han, H. Ishida, Making benzoxazines greener: design, synthesis, and polymerization of a bio-based benzoxazine fulfilling two principles of green chemistry, ACS Sustain. Chem. Eng. J. 6 (2018) 13096–13106.

[38] D.W. Zhao, C. Chen, Q. Zhang, W.S. Chen, S.X. Liu, Q.W. Wang, High performance, flexible, solid-state supercapacitors based on a renewable and biodegradable me-soporous cellulose membrane, Adv. Energy Mater. 7 (18) (2017) 1700739.

[39] F. Chen, Y.J. Zhu, Z.C. Xiong, T.W. Sun, Y.Q. Shen, Highly flexible super-hydrophobic and fire-resistant layered inorganic paper, ACS Appl. Mater. Inter 8 (50) (2016) 34715–34724.

[40] X.Y. Liu, R.H. Zhang, T.Q. Li, P.F. Zhu, Q.X. Zhuang, Novel fully bio-based ben-zoxazines from rosin: synthesis and properties, ACS Sustain. Chem. Eng. J. 5 (11) (2017).

[41] E. Cruz-Valeriano, D.E. Guzmán-Caballero, T. Escamilla-Díaz, A. Gutierrez-Peralta, M. Davila, A. Torres-Ochoa, Dielectric constant measurement using atomic force microscopy of dielectric films: a system theory approach, Appl. Phys. A. 124 (10) (2018) 667.

[42] J. Zhang, C.N. Cao, Evaluation of organic coatings by electrochemical impedance spectroscopy, Corros. Protec. 3 (1998) 99–104.

[43] P. Thirukumaran, R. Sathiyamoorthi, P. Shakila, A.S. Parveen, M. Sarojadevi, New benzoxazines from renewable resources for green composite applications, Polym. Compos. 37 (2) (2016) 573–582.

[44] R. Thirukumaran, P. Sathiyamoorthi, A.S. Shakila, M. Parveen, Synthesis and co-polymerization of fully biobased benzoxazines from renewable resources, ACS Sustain. Chem. Eng. 2 (12) (2014).

[45] F. Kasapoglu, I. Cianga, Y. Yagci, T. Takeichi, Photoinitiated cationic polymeriza-tion of monofunctional benzoxazine, J. Polym. Sci. Pol. Chem. 41 (2003) 3320–3328.

[46] H. Ishida, S. Ohba, Synthesis and characterization of maleimide and norbornene functionalized benzoxazines, Polymer 46 (15) (2005) 5588–5595.

[47] N.K. Sini, J. Bijwe, I.K. Varma, Renewable benzoxazine monomer from vanillin: synthesis, characterization, and studies on curing behavior, J. Polym. Sci. Pol. Chem. 52 (1) (2014) 7–11.

[48] X.B. Shen, L.J. Cao, Y. Liu, J.Y. Dai, X.Q. Liu, S.Y. Du, How does the hydrogen bonding interaction influence the properties of polybenzoxazine? An experimental study combined with computer simulation, Macros. 51 (2018) 4782–4799.

[49] M. Barde, K. Avery, C.W. Edmunds, N. Labbe, M.L. Auad, Cross-Linked acrylic polymers from the aqueous phase of biomass pyrolysis oil and acrylated epoxidized soybean oil, ACS Sustain. Chem. Eng. 7 (2019) 2216–2224.

[50] J.Y. Dai, N. Teng, X.B. Shen, Y. Liu, L.J. Cao, J. Zhu, X.Q. Liu, Synthesis of biobased benzoxazines suitable for vacuum-assisted resin transfer molding process via in-troduction of soft silicon segment, Ind. Eng. Chem. 57 (2018) 3091–3102.

[51] J. Leonhardt, P. Hugo, Comparison of thermokinetic data obtained by isothermal, isoperibolic, adiabatic and temperature programmed measurements, J. Therm. Anal. Calorim. 49 (3) (1997) 1535–1551.

[52] P. Prabunathan, P. Thennarasu, J.K. Song, M. Alagar, Achieving low dielectric, surface free energy and UV shielding green nanocomposites via reinforcing bio-silica aerogel with polybenzoxazine, New J. Chem. 41 (13) (2017).

[53] Y.F. Chen, B.T. Wang, F.L. Li, C.J. Teng, Micro-structure, mechanical properties and dielectric properties of bisphenol a allyl compound-bismaleimide modified by super-critical silica and polyethersulfone composite, J. Electron. Mater. 46 (7) (2017) 4656–4661.

[54] T. Kao, J. Chen, C. Cheng, C.I. Sue, F.C. Chang, Low-surface-free-energy poly-benzoxazine/polyacrylonitrile fibers for biononfouling membrane, Polymer 54 (1) (2013) 258–268.

[55] E. Caldona, A.C. De, B.B. Pajarito, R.C. Advincula, Novel anti-corrosion coatings from rubber-modified polybenzoxazine-based polyaniline composites, Appl. Surf. Sci. 422 (2017).

[56] G.S. Lai, W.J. Lau, P.S. Goh, A.F. Ismail, Y.H. Tan, C.Y. Chong, R. Krause-Rehberg, S. Awad, Tailor-made thin film nanocomposite membrane incorporated with gra-phene oxide using novel interfacial polymerization technique for enhanced water separation, Chem. Eng. J. 344 (2018).

[57] Y.Q. Zhan, J.M. Zhang, X.Y. Wan, Z.H. Long, S.J. He, Y. He, Epoxy composites coating with Fe3O4 decorated graphene oxide: Modified bio-inspired surface chemistry, synergistic effect and improved anti-corrosion performance, Appl. Surf. Sci. 436 (2018) 756–767.

[58] Z. Wang, Q.C. Ran, R.Q. Zhu, Y. Gu, Curing behaviors and thermal properties of

benzoxazine and N, N′-(2, 2, 4-trimethylhexane-1, 6-diyl) dimaleimide blend, J. Appl. Polym. Sci. 129 (3) (2013) 1124–1130.

[59] Y. Liu, Z. Yue, J. Gao, Synthesis, characterization, and thermally activated polymerization behavior of bisphenol-S/aniline based benzoxazine, Polymer 51 (16) (2010) 3722–3729.

[60] J.Y. Dai, N. Teng, X.B. Shen, Y. Liu, L.J. Cao, X.Q. Liu, Synthesis of bio-based benzoxazines suitable for vacuum assisted resin transfer molding (RTM) process via introduction of soft silicon segment, Ind. Eng. Chem. Res. 57 (8) (2018).

[61] M.H. Wang, Q.H. Li, X.G. Li, Y.C. Liu, L.Z. Fan, Effect of oxygen-containing functional groups in epoxy/reduced graphene oxide composite coatings on corrosion protection and antimicrobial properties, Appl. Surf. Sci. 448 (2018) 351–361.

[62] H. Vakili, B. Ramezanzadeh, R. Amini, R. Amini, The corrosion performance and adhesion properties of the epoxy coating applied on the steel substrates treated by cerium-based conversion coatings, Corros. Sci. 94 (2015) 466–475.

[63] K.C. Chang, W.F. Ji, M.C. Lai, Y.R. Hsiao, C.H. Hsu, T.L. Chuang, Correction: synergistic effects of hydrophobicity and gas barrier properties on the anticorrosion property of PMMA nanocomposite coatings embedded with graphene nanosheets, Polym. Chem. 5 (23) (2014) 6865-6865.

[64] C.L. Zhou, X. Lu, Z. Xin, Y.F. Zhang, Intercalated polybenzoxazine/organoclay composites with enhanced performance in corrosion resistance, J. Coat. Technol.

Res. 13 (1) (2016) 63–72.

[65] H. Wei, D.W. Ding, S. Wei, Z.H. Guo, Anticorrosive conductive polyurethane multiwalled carbon nanotube nanocomposites, J. Mater. Chem. 1 (36) (2013) 10805–10813.

[66] S.A. Haddadi, S.A.A. Ramazani, M. Mahdavian, P. Taheri, J.M.C. Mol, Fabrication and characterization of graphene-based carbon hollow spheres for encapsulation of organic corrosion inhibitors, Chem. Eng. J. 352 (2018) 909–922.

[67] D. Prasai, J.C. Tuberquia, R.R. Harl, K. Jennings, Graphene: corrosion-inhibiting coating, ACS Nano 6 (2) (2012) 1102–1108.

[68] D.M. Patil, G.A. Phalak, S.T. Mhaske, Enhancement of anti-corrosive performances of cardanol based amine functional benzoxazine resin by copolymerizing with epoxy resins, Prog. Org. Coat. 105 (2017) 18–28.

[69] Y.W. Ye, Z.Y. Liu, W. Liu, D.W. Zhang, H.C. Zhao, L.P. Wang, X.G. Li, Superhydrophobic oligoaniline-containing electroactive silica coating as pre-process coating for corrosion protection of carbon steel, Chem. Eng. J. 348 (2018) 940–951.

[70] M.T. Mo, W.J. Zhao, Z.F. Chen, E.Y. Liu, Q.J. Xue, Corrosion inhibition of functional graphene reinforced polyurethane nanocomposite coatings with regular texture, RSC Adv. 6 (10) (2016) 7780–7790.